Very large eddy simulation of the vortex rope in the draft tube of Francis turbine

IOP Conf. Series: Earth and Environmental Science **240** (2019) 022001 doi:10.1088/1755-1315/240/2/022001

Very large eddy simulation of the vortex rope in the draft tube of Francis turbine

H Cheng[1,2], L J Zhou[1] and Y Z Zhao[2]

[1]College of Water Conservancy and Civil Engineering, China Agricultural University, No. 17 Tsinghua East Road 100083, Beijing, China

[2]Dongfang Electrical Machinery Co., Ltd., No. 188 Huang He West Road 618000, Deyang, Sichuan Province, China

lodgecheng@163.com

Abstract: There is usually a strong swirling flow between runner and draft tube of Francis turbine at part load, which would lead to a vortex rope in draft tube. RANS and LES models are used by lots of authors to simulate this phenomenon, and the calculated results is almost similar with test observation. However, these turbulent models can't predict the length of helical vortex rope exactly, especially the low pressure and high vorticity in the core of vortex. Very large eddy simulation, as a hybrid RANS-LES methodology, could combine the advantages of RANS and LES, which has been proved by many authors. This paper presents a VLES simulation of draft tube flow field compared with other three turbulence models. The results show that VLES model is able to effectively reduce the eddy viscosity and velocity dissipation in vortex rope field, leading to lower pressure and longer rope than other models Moreover, it is demonstrated that proper mesh is also significant for VLES to predict the cavitation vortex rope observed in model test.

1 Introduction

Most hydraulic turbines are required to operate under part-load condition in order to fulfill variable demands of an electrical grid. There is intense swirling flow subjected to strong curvature, adverse pressure gradient, recirculation between the cone of runner and inlet of draft tube. The draft tube would comprise a shear layer formed around a centrally stalled region directly underneath the nose cone of the runner [1]. A helical vortex, known as the vortex rope, is often formed in the shear layer in draft tube, whose core is a region of low pressure. It sometimes may be lower than the vapor pressure of water and lead to a cavitated vortex rope.

Scherer et al [2], Lipej et al [3] and Foroutan et al [4] use RANS models to calculate flow pattern in the draft tube at part load and get a similar characteristic of vortex rope with experiment observation. They usually use the iso-pressure surface to describe vortex rope, however the calculated pressure is extremely higher than vapor pressure. It could be presumed that the common RANS models could not predict the complex vortices and adverse pressure gradient. Though Guo et al [5], Wu et al [6] and Jošt et al [7] could predict intense vortex in draft tube by LES model, the request of mesh quality is extremely rigorous.

RANS-LES methodology, as a hybrid model, pursued by many researchers is to combine the advantage of RANS and LES in large-scale vortex structures. Speziale [8] firstly rescaled a

conventional RANS model through the introduction of a resolution control function F_r, which modeled the subscale turbulent stress tensor τ_{ij}^{sub} by damping the Reynolds stresses τ_{ij}^{RANS}. That could be expressed by the formulas below. β and n are the constant modeling parameters, Δ is the representative mesh spacing, L_k is the Kolmogorov length scale.

$$\tau_{ij}^{sub} = F_r \tau_{ij}^{RANS} \tag{1}$$

$$F_r = \left[1.0 - exp\left(\frac{-\beta\Delta}{L_k} \right) \right]^n \tag{2}$$

Hsieh et al [9] found that F_r could be written based on the turbulence energy spectrum and had a value between 0 and 1.0 with the final form below. L_c and L_i are the turbulent cut off length scale integral length scale respectively, which have different definitions in different models. Equation (3) constitutes the proposed VLES modeling of the new resolution control function F_r.

$$F_r = \min\left(1.0, \left[\frac{1.0 - exp\left(\frac{-\beta L_c}{L_k} \right)}{1.0 - exp\left(\frac{-\beta L_i}{L_k} \right)} \right]^n \right) \tag{3}$$

2. Turbulence models

The new VLES model was implemented in the general Computational Fluid Dynamics (CFD) code of ANSYS CFX , which is adopted for the numerical study. The VLES modeling are accomplished in the framework of the standard *k-ω* model.

The original standard Wilcox *k-ω* model includes turbulence kinetic energy *k* and specific dissipation *ω*.

$$\frac{\partial(\rho k)}{\partial t} + \frac{\partial}{\partial x_j}(\rho u_j k) = \frac{\partial}{\partial x_j}\left(\left(\mu + \frac{\mu_t}{\sigma_{k1}} \right) \frac{\partial k}{\partial x_j} \right) + P_k - \beta' \rho k \omega \tag{4}$$

$$\frac{\partial(\rho\omega)}{\partial t} + \frac{\partial}{\partial x_j}(\rho u_j \omega) = \frac{\partial}{\partial x_j}[(\mu + \frac{\mu_t}{\sigma_{\omega 1}}) \frac{\partial \omega}{\partial x_j}] + \alpha_1 \frac{\omega}{k} P_k - \beta_1 \rho \omega^2 \tag{5}$$

P_k is the kinetic energy production and μ_t is the turbulent viscosity, as in equation (6) and (9).

$$P_k = \mu_t |S|^2 \tag{6}$$

$$|S| = \sqrt{2 S_{ij} S_{ij}} \qquad S_{ij} = \frac{1}{2}\left(\frac{\partial u_i}{\partial x_j} + \frac{\partial u_j}{\partial x_i} \right) \tag{7-8}$$

$$\mu_t = \rho \frac{k}{\omega} \tag{9}$$

Compared with the standard *k-ω* model, the VLES *k-ω* model only modifies the formulation of the turbulent viscosity [10], as in equation (10).

$$\mu_t = F_r \rho \frac{k}{\omega} \tag{10}$$

There are some parameters associated with the function of F_r, in the form of

$$L_c = C_x (\Delta_x \Delta_y \Delta_z)^{1/3} \qquad L_i = \frac{k^{3/2}}{\beta' k \omega} \qquad L_k = \frac{\nu^{3/4}}{(\beta' k \omega)^{1/4}} \tag{11-12}$$

$$C_x = \sqrt{0.3}\frac{C_s}{\beta'} \qquad C_s = \sqrt{\frac{\left[\left(C_{s,0}^2\Delta^2|S|\right)^2 + \nu^2\right]^{1/2} - \nu}{\Delta^2|S|}} \qquad \Delta = (\Delta_x\Delta_y\Delta_z)^{1/3} \tag{13-15}$$

$C_{s,0}$ is the typical Smagorinsky LES model constant, all the constant modeling parameters as shown in table 2.

Table 1. Model constants for the VLES model.

β	n	β'	α_1	β_1	σ_{k1}	$\sigma_{\omega 1}$	$C_{s,0}$
0.002	2	0.09	5/9	0.075	2	2	0.1

3. Draft tube vortex rope case

The investigated case corresponded to the scale model of a Francis turbine of a specific speed n_s=147 m-kw. The scale model supplied by DFEM (Dongfang Electrical Machinery Co., Ltd.) and the tests were carried out according to the IEC 60193 International Standards. The turbine model had a spiral casing with a stay ring of 24 stay vanes, a distributor made of 24 guide vanes, a runner with 15 blades, and a symmetric elbow draft tube. The runner outlet diameter D_2 was 351 mm, and the net head H of the model test was 30 m. The cone of draft tube was made of the clear acrylic glass, so the behavior of vortex rope at the Thoma number corresponding to the suction height of the prototype power plant could be monitored by using a high speed camera.

This work chose a typical helical rope of draft tube case to validate the numerical simulation, using the dimensionless speed factor n_{11} and discharge factor Q_{11} defined fellow to describe operated point. N was runner rotating speed, D_2 was runner outlet diameter and Q was discharge. The investigated helical vortex rope condition was n_{11}/n_{11opt}=1.1 , Q_{11}/Q_{11opt}=0.9.

$$n_{11} = \frac{ND}{\sqrt{H}} \qquad Q_{11} = \frac{Q}{D_2^{\,2}\sqrt{H}} \tag{16-17}$$

3.1. Boundary condition and numerical settings

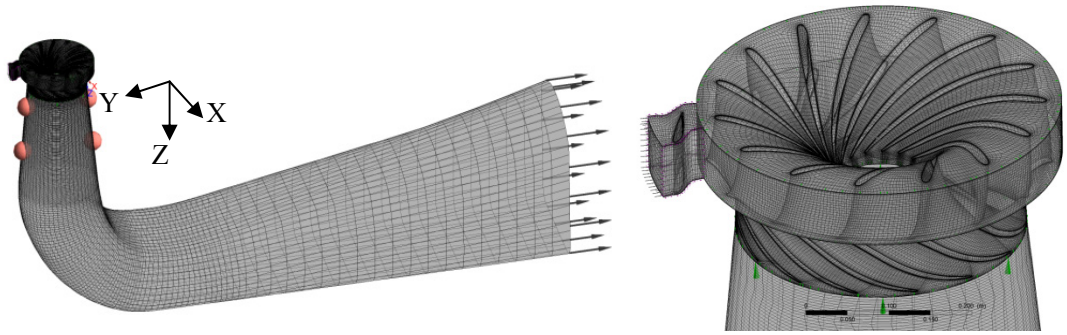

Figure 1. Computational domain and mesh configuration.

The vortex rope at the draft tube depended on the velocity distribution from runner outlet, and the inner flow of runner was influenced by the guide vane outlet flow. Therefore the simulation contained single guide vane, whole runner blades, and a draft tube in the computational domain in figure 1. The transient rotor stator scheme was used to accomplish the rotation and static interface data transmission, and the single guide vane employed the rotational periodicity interface model. The inlet boundary condition was set to total pressure with a flow angle of 38 degree obtained from the whole turbine passage simulation. Static pressure computed through the Thoma number was given at the draft tube outlet, defined in equation (18), and the difference of pressure between inlet and outlet should be 30m.

$$\sigma = \frac{\frac{P_{out}}{\rho g} - h_z - \frac{P_v}{\rho g}}{H} \tag{18}$$

P_{out} was the outlet pressure in draft tube, P_v was the saturated vapor pressure (3540 Pa) and h_z was the suction height benchmarked against the center of guide vane, respectively. Thoma number σ was 0.11, and h_z was about 1 m.

This paper took four different turbulence models to compare with test results, including standard *k-ω*, SAS, VLES and LES. All models would been calculated by unsteady type, using the steady results for initial value. In the simulation, the second order upwind scheme was used for discretization of convective term and the second order central scheme for discretization of diffusion term. The time term in the unsteady simulation was discretized by the second order backward Euler scheme. RMS residual type was chosen as convergence criteria, usually reaching to 1e-05 in most condition. To balance the computational time and accuracy, a time step of 1° runner revolution(Δt =0.000192s) was chosen based on the time independence tests, which was run between 0 and 1.05seconds, averaging the values from 0.5 seconds.

3.2. Mesh scheme and grid scaling test

Three different grid densities (G_1 to G_3) were used to carry out the scaling test, as shown in table 2. The widely accepted grid convergence index (GCI) of Richardson extrapolation method was used to evaluate the numerical uncertainties and grid convergence. The extrapolation values and uncertainty in the grid convergence were estimated using the GCI method. The approximate and extrapolated relative errors as well as grid convergence index were estimated as in equation (19-21), and more details could be gotten from the reference [11].

Table 2. Grid densities used in grid scaling tests.

	G_1	G_2	G_3
Guide vane	21384	21384	21384
Runner	213600	451500	873450
Draft tube	262962	555797	1110424
Total elements	497946	1028681	2005258
Element angle	⩾30.2	⩾32.1	⩾32.8
Expansion factor	⩽58	⩽36	⩽12
Aspect ratio	⩽386	⩽310	⩽273
Averaged Y^+	131	126	122

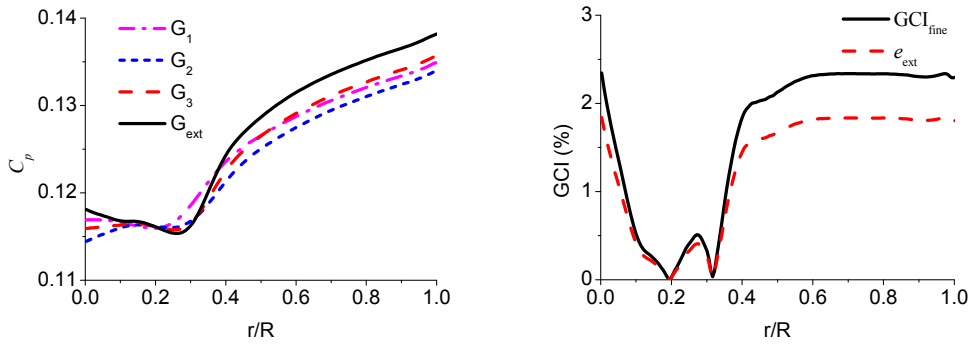

Figure 2. Pressure coefficient and uncertainties GCI index analysis on section of $0.5Z/D_2$.

This estimation was based on unsteady VLES model with the time-averaged results. The critical parameter for the simulation was the averaged pressure coefficient profile, defined in equation (22), in

section of $0.3Z/D_2$. Figure 2 shows the distribution for the different grids . In term of GCI index, the maximum extrapolated relative errors and grid convergence index of VLES were less than 2% and 2.5%, respectively. Therefore, that indexes of VLES could reach the request of Richardson extrapolation method, and G_3 was used in other three models.

$$e_a^{21}=\left|\frac{\phi_1-\phi_2}{\phi_1}\right| \qquad e_{ext}^{21}=\left|\frac{\phi_{ext}^{12}-\phi_1}{\phi_{ext}^{12}}\right| \qquad \mathrm{GCI}_{fine}^{21}=\frac{1.25e_a^{21}}{r_{21}^{p}-1} \tag{19-21}$$

$$C_P=\frac{P\text{-}P_{cav}}{\rho g H} \qquad C_\omega=\frac{\omega_z}{V_{in}/D_2} \tag{22-23}$$

4. Results and discussion

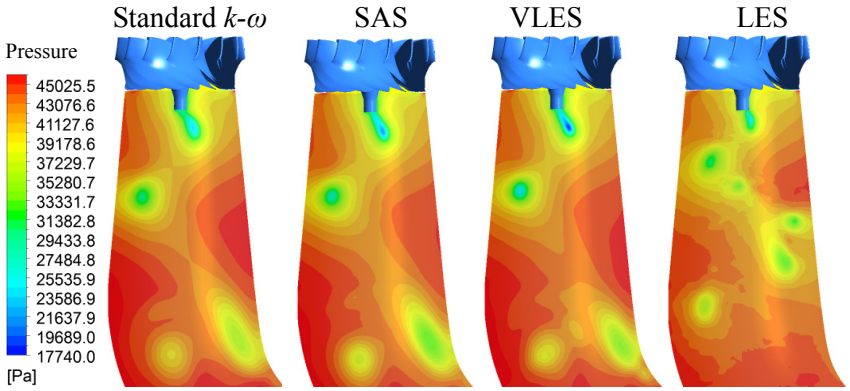

Figure 3. Static pressure distribution on mid-plane.

Figure 3 shows the static pressure distribution at mid-plane of draft tube at t=1.05s. The results from different turbulent models are quite similar except LES, which proves that this simulation can't provide enough mesh density for LES. The pressure calculated by all models is further more than the saturated vapor pressure. However, there is obvious difference for the minimum of static pressure among those models, and VLES get the lowest pressure in the cone. It is concluded that VLES seem to capture the pressure gradient, and the result is more close to saturated vapor pressure than other models.

Figure 4 shows the vortex rope formed in the draft tube at t=1.05 s, visualized by iso-surface contours of pressure for LES and λ_2 =17000 s^-2 for other models. In order to research further the draft vortex, this paper would analyze the flow pattern of different sections at Z/D_2=0.2, 0.3, 0.4, 0.6, 0.8, 1, 1.25 ,1.5. It is observed that though all the calculated vortex ropes have similar shape compared with experimental observation, there is a notable difference for the length of rope. The vortex rope from standard *k-ω* is quite short, proving that the fluid field is not developed enough. Turning to the SAS and VLES cases, the rope tail seems to be well extended to downstream, and the rope length increases from $0.66D_2$ to $0.99D_2$ and $1.1D_2$ respectively. Though the calculated rope length is less than the test result, it can be concluded that VLES could simulate the intense turbulence flow and vortex rope length exactly in the draft tube.

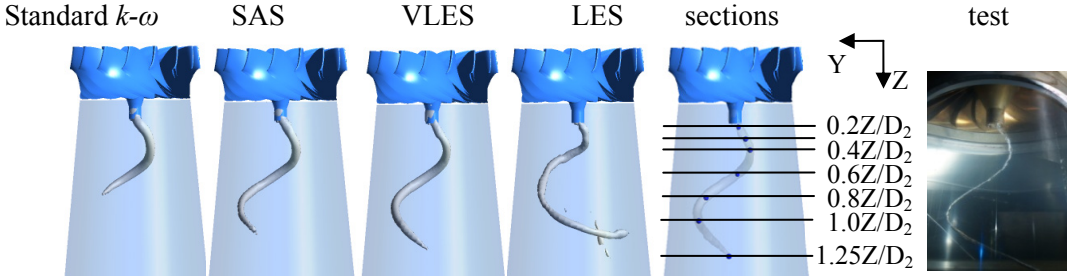

Figure 4. Snapshot of the vortex rope visualized by iso-surface contours.

Figure 5 shows the static pressure and vorticity at these sections, and the results from standard *k-ω*, SAS, VLES are quite similar. Due to the intense rotation of flow, high pressure and low vorticity are concentrated in the core of vortex rope. In cases with the pressure and vorticity coefficient of vortex core at different sections, as shown in figure 6, the pressure coefficient C_p increases from upstream to downstream, and the vorticity coefficient C_w has a opposite trend, defined in equation (22). It could be concluded that the rotation intensity of flow is gradually weaken, and the character of rope vanishes along with the vortex breakdown. Though the standard *k-ω* and SAS could predict a similar trend with VLES, there are some differences among those models. Comparing with VLES, C_p of other two models are always higher by 25% and 12%, and C_w are lower by 35% and 10% respectively. VLES seems to provide a lower static pressure and higher vorticity in the core of vortex rope, which proves that VLES is good at simulating the vortex rope flow.

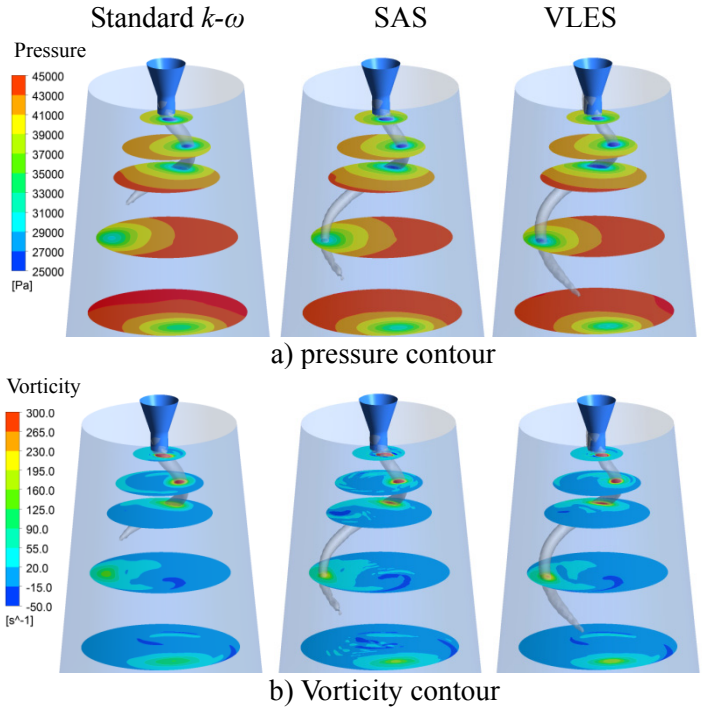

a) pressure contour

b) Vorticity contour

Figure 5. Static pressure and vorticity contour on different sections.

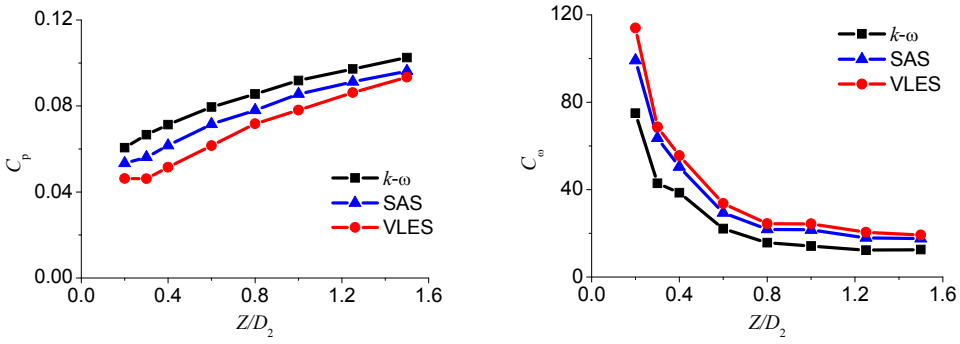

a) Pressure coefficient b) Vorticity coefficient

Figure 6. Static pressure and vorticity coefficient from upstream to downstream.

In addition, the turbulent viscosity is only modified in the VLES *k-ω* model, as in equation (19), which should be compared with other models. Figure 7 shows that the eddy viscosity obtained from standard *k-ω* rises with the vortex rope developing to downstream, especially around the core of rope.

However, SAS predicts that the vortex rope becomes longer than standard *k-ω* only by decreasing the eddy viscosity in the core of rope. What's more, VLES keeps reducing the eddy viscosity and velocity dissipation of the whole flow field, which leads vortex rope extending to the further downstream. In terms of the eddy viscosity value, as shown in figure 8, μ_t obtained from SAS or VLES almost decreases to one quarter or one percent of the standard *k-ω* case. It could be concluded that reducing the eddy viscosity is helpful to gain low static pressure of vortex core and long vortex rope.

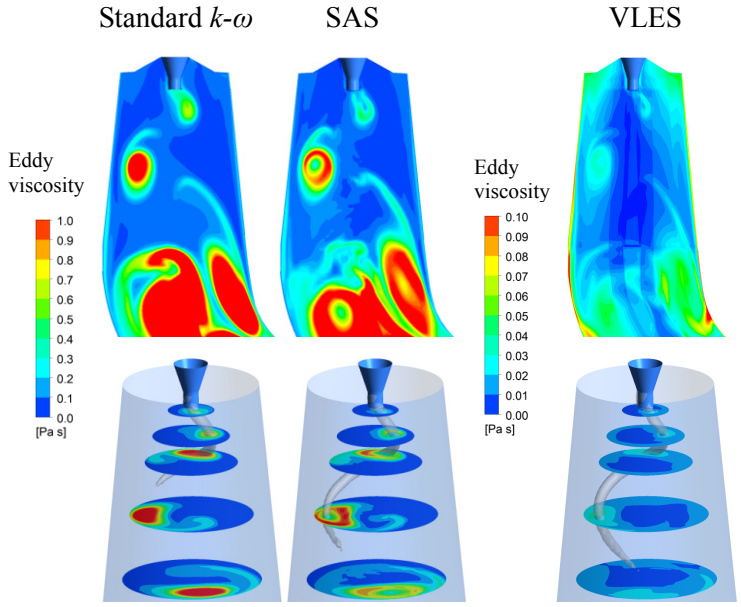

Figure 7. Eddy viscosity contour on different sections.

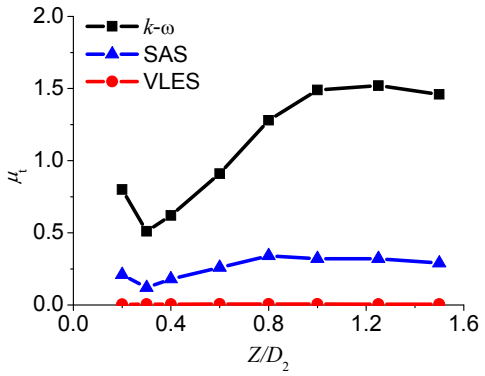

Figure 8. Eddy viscosity value from upstream to downstream.

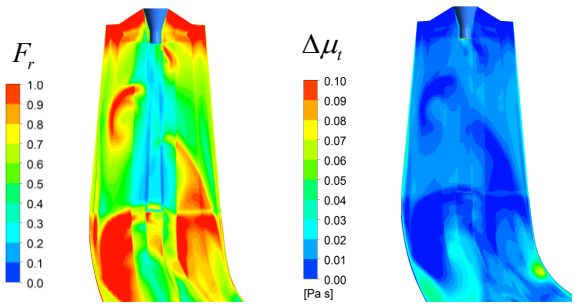

Figure 9. Modification of eddy viscosity for VLES (left: Fr, right: $\Delta\mu_t$).

The coefficient F_r is low in the center of vortex rope, as shown in figure 9, representing a high

modification of eddy viscosity, and $\Delta\mu_t$ is the difference of eddy viscosity modified by F_r. VLES could exactly identify the vortex core, and modify effectively the turbulent variables in the draft tube. Meanwhile, the size of mesh has a significant effect on the distribution of F_r, therefore, it's very important to make the mesh to be uniform and proper.

Though VLES is helpful to simulate the vortex rope to some extent, the minimal pressure in the vortex core is much higher than the saturated vapor pressure, which is not accord with the observation in test. As a result, this paper continues to increase the grid density of draft tube, and the elements of another three cases(G_4, G_5, G_6) are shown in table 3. It could be found that the low pressure part is more distinct with the rise of grid number, proving that the mesh plays an important role in simulating the draft vortex rope, as shown in figure 10. What's more, the length of vortex rope also grows from $1.1D_2$ to $1.8D_2$ and reach to the elbow part of draft tube. Due to the limit of tube wall, the vortex rope gradually breaks down and forms lots of small-scale vortices, which is consistent with the fact. Figure 11 shows that the pressure coefficient of vortex core on each section decreases with the mesh increasing, and the vorticity coefficient has a opposite trend. This change for pressure coefficient is notable from G5 to G6, and almost disappeared after the $0.6Z/D_2$ section. The pressure of vortex core has already been lower than the saturated vapor pressure before $0.3Z/D_2$, indicating that water in this part would be changed to vapor. This change for vorticity coefficient is also obvious especially at the inlet of draft tube, and goes to convergence when grid number continues to increase.

Table 3. Information of grid densities increasing.

	G_4	G_5	G_6
Guide vane	21384	21384	21384
Runner	873450	873450	873450
Draft tube	2400004	4939296	10026953
Total elements	3294838	5834130	10921787
Averaged Yplus	114	103	76

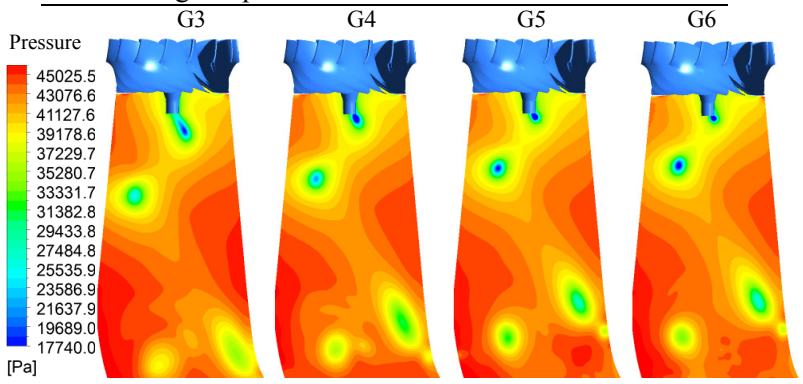

a) pressure contour

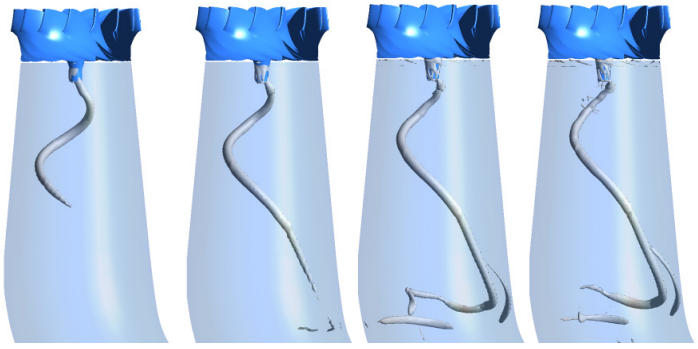

b) vortex rope iso-contour（λ_2=17000 s^-2）

Figure 10. Flow structure for VLES with the grids increase.

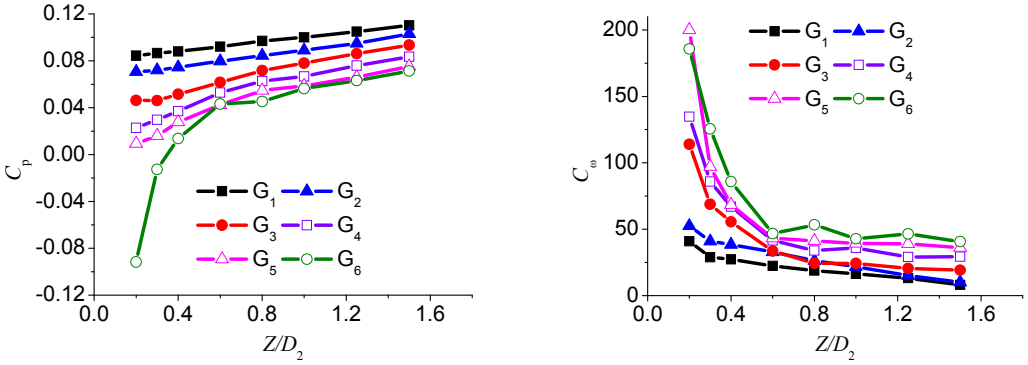

a) Pressure coefficient b) Vorticity coefficient

Figure 11. Static pressure and vorticity coefficient obtained from VLES with different grids.

5. Conclusions

Numerical simulation of turbulent flow in draft tube is performed in this study. Unsteady simulations for vortex rope are carried out using four different turbulence models, which is compared with experimental observation. Though the regular RANS models can simulate unsteadiness flow field caused by helical vortex ropes, VLES is able to capture lower pressure and longer rope in the draft tube. What's more, enough grids are helpful for VLES to calculate minimal pressure in the core of vortex rope. It could be concluded that effective turbulent model and proper mesh are significant to predict the cavitation vortex rope observed in model test. For further improvement of the simulation results the use of two-phase models should be investigated in the future.

Acknowledgements

The research presented in this work was supported by National Natural Science Foundation of China (NO:51479200).

References

[1] Nishi M and Liu S H 2012 *Proc. Int. Conf. on 26th IAHR Symposium on Hydraulic Machinery and Systems* (*China*)
[2] Scherer T, Faigle P and Aschenbrenner T 2002 *Proc. Int. Conf. on 21st IAHR Symposium on Hydraulic Machinery and Systems (Lausanne Switzerland)*
[3] Lipej A, Jošt D, Meznar P 2008 *Proc. Int. Conf. on24th IAHR Symposium on Hydraulic Machinery and Systems (Foz Do Iguassu)*
[4] Foroutan H, Yavuzkurt S. 2012 *Proc. Int. Conf. on the 26nd IAHR Symposium(Beijing, China)*
[5] Guo Y, Kato C and Miyagawa K 2006 *Proc. Int. Conf. on23rd IAHR Symposium on Hydraulic Machinery and Systems (Yokohama Japan)*
[6] Wu X J, Liu S H and Wu Y L 2006 *Proc. Int. Conf. on23rd IAHR Symposium on Hydraulic Machinery and Systems (*Yokohama Japan*)*
[7] Jošt D and Lipej A 2011 *J. of Mech. Eng.* **57** 445
[8] Speziale C G 1998 *AIAA Journal* **36** 173
[9] Hsieh K J, Lien F S and Yee E 2010 *Flow Turbulence and Combustion* **84** 193
[10] Han X S and Krajnović S 2015 *AIAA Journal* **4** 1103
[11] Celik I B, Ghia U and Roache P J 2008 *J. of Fluids Eng.* **7** 1